Orbit optimization and time delay interferometry for inclined ASTROD-GW formation with half-year precession-period

Wang Gang(王 刚)[a)†] and Ni Wei-Tou(倪维斗)[b)‡]

[a)] *Shenzhen National Climate Observatory, Shenzhen* 518040, *China*

[b)] *Center for Gravitation and Cosmology (CGC), Department of Physics, Tsing Hua University, Hsinchu, Taiwan* 30013, *China*

(Received 15 September 2014; revised manuscript received 18 December 2014; published online 2 April 2015)

ASTROD-GW (ASTROD [astrodynamical space test of relativity using optical devices] optimized for gravitational wave detection) is a gravitational-wave mission with the aim of detecting gravitational waves from massive black holes, extreme mass ratio inspirals (EMRIs) and galactic compact binaries together with testing relativistic gravity and probing dark energy and cosmology. Mission orbits of the 3 spacecrafts forming a nearly equilateral triangular array are chosen to be near the Sun–Earth Lagrange points L3, L4, and L5. The 3 spacecrafts range interferometrically with one another with arm length about 260 million kilometers. For 260 times longer arm length, the detection sensitivity of ASTROD-GW is 260 fold better than that of eLISA/NGO in the lower frequency region by assuming the same acceleration noise. Therefore, ASTROD-GW will be a better cosmological probe. In previous papers, we have worked out the time delay interferometry (TDI) for the ecliptic formation. To resolve the reflection ambiguity about the ecliptic plane in source position determination, we have changed the basic formation into slightly inclined formation with half-year precession-period. In this paper, we optimize a set of 10-year inclined ASTROD-GW mission orbits numerically using ephemeris framework starting at June 21, 2035, including cases of inclination angle with 0° (no inclination), 0.5°, 1.0°, 1.5°, 2.0°, 2.5°, and 3.0°. We simulate the time delays of the first and second generation TDI configurations for the different inclinations, and compare/analyse the numerical results to attain the requisite sensitivity of ASTROD-GW by suppressing laser frequency noise below the secondary noises. To explicate our calculation process for different inclination cases, we take the 1.0° as an example to show the orbit optimization and TDI simulation.

Keywords: orbit optimization, ASTROD-GW, gravitational wave detector, time delay interferometry

PACS: 95.10.Eg, 95.55.Ym, 04.80.Nn, 07.60.Ly **DOI:** 10.1088/1674-1056/24/5/059501

1. Introduction

Gravitational wave (GW) detection will provide a new method to probe astrophysics, cosmology, and fundamental physics. The experimental GW communities in the world are actively looking forward to the rise of experimental GW astronomy and cosmology.[1,2] Cosmic microwave background (CMB) polarization observation teams are actively looking for B-mode polarization imprints from primordial/inflationary GWs.[3–7] The real-time GW detectors at present are mainly ground-based interferometers and pulsar timing arrays (PTAs). The second-generation ground-based interferometers seeking to detect GWs in the high frequency band under active construction are advanced LIGO,[8] advanced Virgo[9] and KAGRA/LCGT.[10] LIGO-India is under active consideration.[11,12] PTAs seek for detection of GWs from supermassive black hole (SMBH) merger events and stochastic background in the very low frequency band (300 pHz–100 nHz).[13–16] Prospects for real-time detection of GWs before or around 2020 are promising.

To detect GWs from various different astrophysical and cosmological sources in different spectral ranges and to enhance the signal to noise ratios, we need to explore the GW spectrum between the high-frequency band and the very low-frequency band, i.e., the middle frequency band (0.1 Hz–10 Hz) and the low frequency band (100 nHz–0.1 Hz).[1,2,17] Space detectors are most sensitive to these bands. Mission concepts under implementation and study are eLISA/NGO,[18] ASTROD-GW,[1,17,19–21] Super-ASTROD,[22] BBO,[23] and DECIGO.[24–26] Except for the Fabry–Perot implementation of DECIGO whose scheme is in principle like the ground-based GW interferometric detectors, all other missions have unequal arm lengths and the laser frequency noise needs very serious consideration. One way to suppress it is to use time delay interferometry (TDI) by combining paths to make the two interfering beam to have closely equal optical paths. Time delay interferometry is considered for ASTROD in 1996[27,28] and has been worked out for LISA much more thoroughly since 1999.[29,30]

In our recent papers, we have worked out various TDI configurations numerically for ASTROD-GW,[31–34] LISA,[35] and eLISA/NGO[36] and compared them with one

†Corresponding author. E-mail: gwanggw@gmail.com

‡Corresponding author. E-mail: weitou@gmail.com

© 2015 Chinese Physical Society and IOP Publishing Ltd

another.[21] These second generation TDIs all satisfy their respective requirements. In the previous ASTROD-GW orbit configuration, we have used the ecliptic plane orbit formation in the original proposal. The angular position in the sky has a binary reflection ambiguity above and below the ecliptic plane. The resolution is poor when the source is near the ecliptic poles. Subsequently we have redesigned the basic orbits of ASTROD-GW configuration to have small inclinations with respect to the ecliptic plane to resolve these issues while keeping the variation of the arm lengths in the acceptable range.[17,21] In the present paper, we work out a set of 10-year optimized ASTROD-GW mission orbit configurations using numerical ephemeris, and calculate the residual optical path differences in the first and second generation TDIs for these inclined configurations. In our optimized mission orbits of ASTROD-GW for 10 years with 0° (no inclination), 0.5°, 1.0°, 1.5°, 2.0°, 2.5°, 3.0° inclined angles, changes of arm length are less than 0.0006, 0.0006, 0.0007, 0.0010, 0.0013, 0.0018, 0.0024 AU respectively; the Doppler velocities between each two S/Cs of the three arms are less than 3, 4, 10, 20, 34, 51, 73 m/s respectively; the rms (root-mean-square) Doppler velocities are about 1.2, 1.7, 5.6, 12.5, 22, 35, 50 m/s respectively. All the second generation TDIs considered for one-detector case with no inclination and with 0.5° inclination satisfy the original ASTROD-GW requirement on TDI path difference of less than 1.5 μs. For the case of 1.0° inclination, there are 10 second generation TDIs satisfy the requirement of mission in the 14 configurations calculated. For the cases of 1.5° to 3°, the requirement needs to be relaxed by 6 to 25 times; that is, the laser frequency stabilization noise needs to be suppressed by this additional factor. Among the first generation TDIs considered, the requirement for unequal arm Michelson, Relay, Beacon, and Monitor needs to be relaxed by 1–3 orders. With the present pace of development, the laser frequency stabilization requirement for space equipment is expected to be able to compensate for this TDI requirement relaxation 20 years later.

In Section 2, we review the basic inclined ASTROD-GW formation with half-year precession-period. In Section 3, we use the CGC 2.7.1 ephemeris framework to optimize the mission orbit design numerically for ASTROD-GW formation to have nearly equal arm lengths and to have minimal line-of-site Doppler velocity between different pairs of spacecrafts for 10 years, including the cases of inclination angle 0.5°, 1°, 1.5°, 2°, 2.5°, and 3° with respect to the ecliptic plane. In November 2013, ESA announced the selection of the Science Themes for the L2 and L3 launch opportunities – the "Hot and Energetic Universe" for L2 and "The Gravitational Universe" for L3.[37] ESA L3 mission is likely to have a launch opportunity in 2034.[37] Since eLISA/NGO GW mission concept is the major candidate at this time and it takes one year to transfer to the science orbit, a starting time for science phase is likely in 2035. We take the starting time at June 21, 2035 to conform to the general trend of expectation of GW missions for the orbit design and the TDI simulation of science phase of ASTROD-GW with inclined orbit configurations. Since the design and simulation is for 10 years, if the starting time is before 2040, it could be used as a design and simulation for a five-year mission or more. To facilitate comparison, we also work out orbit configuration with no inclination at this starting time. In Section 4, we calculate the TDIs for these ASTROD-GW orbit configurations. Section 4.1 summarizes the basics of time-delay interferometry. In Section 4.2, we work out the first generation TDIs for ASTROD-GW numerically. In Section 4.3, we work out the second generation TDIs for ASTROD-GW with one interferometer and two arms. In Section 5, we conclude this paper with discussion.

2. Basic orbit design of the ASTROD-GW formation with inclination

In this section, we review and summarize the basic inclined mission formation for ASTROD-GW.

The mission configuration of ASTROD-GW is to have its 3 spacecrafts to form a nearly equilateral triangular array with each S/C near one of the Sun–Earth Lagrange points L3, L4, and L5 respectively focusing on GW detection at low frequency. In the original proposal, the ASTROD-GW orbits are chosen in the ecliptic plane, i.e. the inclination $\lambda = 0$ (no inclination). For GW detection, the source angular position determination in the sky has reflection ambiguity above and below the ecliptic plane. The original ASTROD-GW proposal has poor angular resolution near the ecliptic poles, although the resolution is good for the most of sky direction. Now we have redesigned the basic orbits of ASTROD-GW to have small inclinations to resolve these issues while keeping the variation of the arm lengths in the acceptable range.[17,21]

The basic idea of the redesign is as follows. If the orbits of the ASTROD-GW spacecraft are inclined with a small angle λ, the interferometry plane with appropriate design is also inclined with a similar angle. When the ASTROD-GW formation evolves, the interferometry plane can be designed to precess in the ecliptic solar-system barycentric frame with a half-year period. For continuous or quasi-continuous GW sources both near the polar region and off the polar region, the angular positions will be resolved without reflection ambiguity.

The basic configuration uses inclined circular orbit in the heliocentric ecliptic coordinate system. The orbit equation for an inclined circular orbit is[17,21]

$$\begin{pmatrix} x' \\ y' \\ z' \end{pmatrix} = \begin{pmatrix} a\left[1-\sin^2\Phi_0\,(1-\cos\lambda)\right]\cos\varphi + a\sin\Phi_0\cos\Phi_0\,(1-\cos\lambda)\sin\varphi \\ a\cos\Phi_0\sin\Phi_0\,(1-\cos\lambda)\cos\varphi + a\left[1-\cos^2\Phi_0\,(1-\cos\lambda)\right]\sin\varphi \\ -a\sin\Phi_0\sin\lambda\cos\varphi + a\cos\Phi_0\sin\lambda\sin\varphi \end{pmatrix}, \tag{1}$$

where λ is the inclination angle, Φ_0 is the right ascension of ascending node (RAAN), and $\varphi = \omega t + \varphi_0$ with $\varphi - \Phi_0$ the true anomaly and a the semi-major axis corresponding to the mean motion ω of 1 rev/sidereal year.[17,21]

For the three orbits with inclination λ (in radian) in the convention used in this paper (the numbering of S/C2 and S/C3 is switched compared with that of Refs. [17] and [21], i.e. S/C2 $\leftrightarrow$ S/C3; this applies to all the formulas), we have

$$\begin{aligned} &\mathrm{S/C1}: \quad \Phi_0(1) = 270^\circ, \quad \varphi_0(1) = 0^\circ; \\ &\mathrm{S/C2}: \quad \Phi_0(2) = 30^\circ, \quad \varphi_0(2) = 240^\circ; \\ &\mathrm{S/C3}: \quad \Phi_0(3) = 150^\circ, \quad \varphi_0(3) = 120^\circ. \end{aligned} \tag{2}$$

Defining

$$\xi \equiv 1 - \cos\lambda = 0.5\lambda^2 + \mathrm{O}\left(\lambda^4\right), \tag{3}$$

we have explicitly the follows:

(i) For the orbit of S/C1,

$$\begin{pmatrix} x_1 \\ y_1 \\ z_1 \end{pmatrix} = \begin{pmatrix} a\cos\omega t - a\xi\cos\omega t \\ a\sin\omega t \\ a\cos\omega t\sin\lambda \end{pmatrix}. \tag{4}$$

(ii) For the orbit of S/C2,

$$\begin{pmatrix} x_2 \\ y_2 \\ z_2 \end{pmatrix} = \begin{pmatrix} a[(-1/2)\cos\omega t - (3^{1/2}/2)\sin\omega t] + (a/2)\xi[(3^{1/2}/2)\sin\omega t - (1/2)\cos\omega t] \\ a[(-1/2)\sin\omega t + (3^{1/2}/2)\cos\omega t] + \left(3^{1/2}/2\right)a\xi[(3^{1/2}/2)\sin\omega t - (1/2)\cos\omega t] \\ a\sin\lambda[(3^{1/2}/2)\sin\omega t - (1/2)\cos\omega t] \end{pmatrix}. \tag{5}$$

(iii) For the orbit of S/C3,

$$\begin{pmatrix} x_3 \\ y_3 \\ z_3 \end{pmatrix} = \begin{pmatrix} a[(-1/2)\cos\omega t + (3^{1/2}/2)\sin\omega t] + (a/2)\xi[(3^{1/2}/2)\sin\omega t - (1/2)\cos\omega t] \\ a[(-1/2)\sin\omega t - (3^{1/2}/2)\cos\omega t] - (3^{1/2}/2)a\xi[(-3^{1/2}/2)\sin\omega t - (1/2)\cos\omega t] \\ a\sin\lambda[(-3^{1/2}/2)\sin\omega t - (1/2)\cos\omega t] \end{pmatrix}. \tag{6}$$

Figure 1 shows the orbits in three dimension for inclination $\lambda = 1^\circ$ case with the scale of z axis blowing up by tenfold. With Eqs. (4)–(6), the arm lengths are calculated to be

$$\begin{aligned} |\boldsymbol{V}_{2-1}| &= 3^{1/2}a\left[(1-\xi/2)^2 + \sin^2\lambda\sin^2(\omega t - 60^\circ)\right]^{1/2}, \\ |\boldsymbol{V}_{3-2}| &= 3^{1/2}a\left[(1-\xi/2)^2 + \sin^2\lambda\sin^2(\omega t)\right]^{1/2}, \\ |\boldsymbol{V}_{1-3}| &= 3^{1/2}a\left[(1-\xi/2)^2 + \sin^2\lambda\sin^2(\omega t + 60^\circ)\right]^{1/2}. \end{aligned} \tag{7}$$

The fractional arm length variation is within $\pm(1/2)\sin^2\lambda$, e.g., $\pm 0.76\times10^{-4}$ for $\lambda = 1^\circ$.

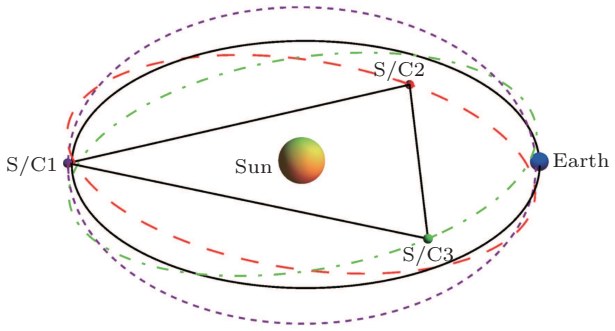


Fig. 1. (color online) Schematic diagram of ASTROD-GW mission orbit design with inclination.

The Doppler velocity (line-of-sight velocity) between two spacecrafts, e.g., S/C2 and S/C3 is

$$\begin{aligned} \frac{\mathrm{d}|\boldsymbol{V}_{3-2}|}{\mathrm{d}t} &= (3^{1/2}/2)a\omega\sin^2\lambda\sin(2\omega t)[(1-\xi/2)^2 \\ &\quad + \sin^2\lambda\sin^2(\omega t)]^{-1/2}. \end{aligned} \tag{8}$$

From this equation the line-of-sight Doppler velocity is less than $(3^{1/2}/2)a\omega\sin^2\lambda(1+\mathrm{O}(\lambda^2))$.

The fractional arm length variations, arm length variations, and Doppler velocity variations for the basic configurations of ASTROD-GW for 10 years respectively with the inclination angle 0° (no inclination), 0.5°, 1°, 1.5°, 2°, 2.5°, and 3° to the ecliptic plane are listed in columns 2–4 in Table 1. In Section 3 we do orbit optimization to these formations with starting time at June 21, 2035 (JD2464500.0) including planetary perturbations. Their values of Doppler velocity variations and arm length variations in 10 years are listed in columns 5 and 6 of Table 1.

The cross-product vector $\boldsymbol{N}(t) \equiv \boldsymbol{V}_{3-2}\times\boldsymbol{V}_{1-3}$ is normal to the orbit configuration plane and has the following components:

$$\boldsymbol{N} = (3^{3/2}/2)a^2(1-\xi/2)\begin{pmatrix} -\sin\lambda\cos2\omega t \\ -\sin\lambda\sin2\omega t \\ 1-\xi/2 \end{pmatrix}. \tag{9}$$

Table 1. Inclined ASTROD-GW formations, arm length variation, and Doppler velocity variations.

Nominal orbit inclination λ	Fractional arm length variation (2 body gravitational field)	Arm length variation (2 body gravitational field)	Doppler velocity variation (2 body gravitational field)	Simulated Doppler velocity variation with planetary perturbations (10 years)	Simulated arm length variation with planetary perturbations (10 years)
0°	0	0	0	3 m/s	6×10^{-4} AU
0.5°	0.19×10^{-4}	0.33×10^{-4} AU	2.0 m/s	4 m/s	6×10^{-4} AU
1°	0.76×10^{-4}	1.32×10^{-4} AU	7.9 m/s	10 m/s	7×10^{-4} AU
1.5°	1.71×10^{-4}	2.97×10^{-4} AU	18 m/s	20 m/s	10×10^{-4} AU
2°	3.04×10^{-4}	5.27×10^{-4} AU	32 m/s	34 m/s	13×10^{-4} AU
2.5°	4.75×10^{-4}	8.23×10^{-4} AU	49 m/s	51 m/s	18×10^{-4} AU
3°	6.84×10^{-4}	11.8×10^{-4} AU	71 m/s	73 m/s	24×10^{-4} AU

The normalized unit normal vector $\boldsymbol{n}$ is then

$$\boldsymbol{n}=\left[\sin^2\lambda+(1-\xi/2)^2\right]^{-1/2}\begin{pmatrix}-\sin\lambda\cos2\omega t\\-\sin\lambda\sin2\omega t\\1-\xi/2\end{pmatrix}. \quad (10)$$

Thus, the ASTROD-GW formation precesses with angular velocity 2ω, i.e., with precession period half sidereal year.

The geometric center $\boldsymbol{V}_{\rm c}$ of the ASTROD-GW spacecraft configuration is

$$\boldsymbol{V}_{\rm c}=\begin{pmatrix}-(1/2)a\xi\cos\omega t\\(1/2)a\xi\sin\omega t\\0\end{pmatrix}. \quad (11)$$

There are 3 interferometers with 2 arms in the ASTROD-GW configuration. The geometric centers of these 3 interferometers are at a distance of about 0.25 AU from the Sun. For 6 inclinations between 0.5° to 3°, we optimize their orbit configurations and simulate various TDI numerically using planetary ephemeris to take into account the planetary perturbations. When eLISA formation orbits around the Sun, it is equivalent to multiple detector arrays distributed in 1 AU orbit. The extension of ASTROD-GW is already of 1 AU. When ASTROD-GW formation orbits around the Sun, it is also equivalent to multiple detector arrays distributed in 1 AU orbit. For its angular resolution compared with eLISA, see Refs. [17] and [21].

3. Mission orbit optimization

The goal of ASTROD-GW mission orbit optimization is to equalize the three arm lengths of ASTROD-GW formation and to reduce the relative line-of-sight velocities between three pairs of spacecrafts as much as possible in realistic situation with planetary perturbations. In the solar system the periods and eccentricities of the ASTROD-GW spacecraft orbits are perturbed by the other planets with largest caused by Jupiter and Venus. Our method of optimization is to modify the initial velocities and initial heliocentric distances so that the perturbed orbital periods for ten-year average remain close to a sidereal year and the average eccentricities remain near zero. In our first optimization, the start time of the science part of the mission is chosen to be June 21, 2025 (JD2460848.0) and the optimization is for a period of 3700 days.[38,39] Since the preparation of the mission may take longer time, in our second optimization, we start at noon, June 21, 2028 (JD2461944.0) and optimize for a period of 20 years for doing numerical TDIs.[31–34] In this paper, we optimize the orbit configurations of ASTROD-GW for 10 years for the cases with the inclination angle 0.5°,1°, 1.5°, 2°, 2.5°, and 3° to the ecliptic plane starting at noon, June 21, 2035 (JD2464500.0) for reason explained in the Introduction. For reference, we also do the optimization for no inclination case.

We calculate and optimize the realistic orbit configurations by using the CGC 2.7.1 ephemeris. In our previous paper,[34] we used the CGC 2.7 ephemeris. The differences between CGC 2.7.1 and CGC 2.7 are detailed in Section 3.1. In Section 3.2, we obtain the initial choice of S/C initial conditions as a starting point for optimization. In Section 3.3, we discuss method of optimization. In Section 3.4, we present the results of optimization.

3.1. CGC 2.7.1 ephemeris

Modern ephemerides are built upon the post-Newtonian dynamics.[40–42] The CGC ephemeris use the post-Newtonian equations given by Brumberg.[43] In the CGC 2.7.1 ephemeris framework, we pick up 340 asteroids besides the Ceres, Pallas, and Vesta from the Lowell database.[44] The masses of 340 asteroids are given by DE430/DE431[45] instead of estimating the masses based on the classification in CGC 2.7.[34–36] The orbit elements of these asteroids are also updated from the Lowell database.

For a 10-year duration starting at June 21, 2035, the differences between the Earth's heliocentric distances calculated by CGC 2.7.1 and DE430 are within 150 m, and the differences in longitudes and latitudes are within 1.4 mas and 0.45 mas respectively. These differences will not affect the results of our TDI calculations.

3.2. Initial choice of spacecraft initial conditions

The R. A. of the Earth at JD2464500 (2035-June-21st 12:00:00) is $17^{h}57^{m}45.09^{s}$, i.e. 269.438° from DE 430 ephemeris. The initial positions of the 3 S/Cs are obtained by choosing the ωt as 89.44° for $\varphi = \omega t + \varphi_0$ in Eq. (1). The initial velocities are derived from Eq. (1) by calculating the derivatives with respect to t. The S/C1 near the Lagrange point L3 is partly obscured by Sun from the line of sight of Earth (Fig. 2(a)). It would obstruct the communication with the Earth stations. To avoid the obscuration, we rotate the initial angle Φ_0 and φ_0 forward of by 2.8°, 2.4°, 2.0°, 1.8°, 1.4°, 1.3°, and 1.2° for inclination angle 0.0° 0.5°, 1.0°, 1.5°, 2.0°, 2.5°, and 3.0° respectively. For the case with inclination angle 1.0°, the S/C1 orbit is shown in Fig. 2(b). The initial choice of initial states for the 3 S/Cs in this case is listed in column 3 of Table 2.

Table 2. Initial states of S/Cs for the configuration with the inclination angle 1° at epoch JD2464500.0 for initial choice, after period optimization, and after all optimizations in J2000 equatorial solar-system-barycentric coordinate system.

$\lambda = 1.0°$		Initial choice of S/Cs initial states	Initial states of S/Cs after period optimization	Initial states of S/Cs after final optimization
S/C1 position/AU	X	$-2.8842263289715 \times 10^{-2}$	$-2.8842263289715 \times 10^{-2}$	$-2.8842514605546 \times 10^{-2}$
	Y	$9.1157742309044 \times 10^{-1}$	$9.1157742309044 \times 10^{-1}$	$9.1158659433458 \times 10^{-1}$
	Z	$3.9552690922456 \times 10^{-1}$	$3.9552690922456 \times 10^{-1}$	$3.9553088730467 \times 10^{-1}$
S/C1 velocity/(AU/day)	V_x	$-1.7188548244458 \times 10^{-2}$	$-1.7188535691176 \times 10^{-2}$	$-1.7188363750567 \times 10^{-2}$
	V_y	$-2.8220395391983 \times 10^{-4}$	$-2.8220375159556 \times 10^{-4}$	$-2.8220098038726 \times 10^{-4}$
	V_z	$-4.4970276654173 \times 10^{-4}$	$-4.4970243993363 \times 10^{-4}$	$-4.4969796642665 \times 10^{-4}$
S/C2 position/AU	X	$8.7453598387569 \times 10^{-1}$	$8.7453598387569 \times 10^{-1}$	$8.7453598387569 \times 10^{-1}$
	Y	$-4.3802677355114 \times 10^{-1}$	$-4.3802677355114 \times 10^{-1}$	$-4.3802677355114 \times 10^{-1}$
	Z	$-2.0634980179207 \times 10^{-1}$	$-2.0634980179207 \times 10^{-1}$	$-2.0634980179207 \times 10^{-1}$
S/C2 velocity/(AU/day)	V_x	$8.2301784322477 \times 10^{-3}$	$8.2301033726700 \times 10^{-3}$	$8.2301033726700 \times 10^{-3}$
	V_y	$1.3797379424198 \times 10^{-2}$	$1.3797253460590 \times 10^{-2}$	$1.3797253460590 \times 10^{-2}$
	V_z	$6.1425805519808 \times 10^{-3}$	$6.1425244722884 \times 10^{-3}$	$6.1425244722884 \times 10^{-3}$
S/C3 position/AU	X	$-8.5683596527799 \times 10^{-1}$	$-8.5683596527799 \times 10^{-1}$	$-8.5679330969623 \times 10^{-1}$
	Y	$-4.8998222347472 \times 10^{-1}$	$-4.8998222347472 \times 10^{-1}$	$-4.8995800210059 \times 10^{-1}$
	Z	$-1.9592963105165 \times 10^{-1}$	$-1.9592963105165 \times 10^{-1}$	$-1.9591994878015 \times 10^{-1}$
S/C3 velocity/(AU/day)	V_x	$8.9788714330506 \times 10^{-3}$	$8.9787977300014 \times 10^{-3}$	$8.9792464008067 \times 10^{-3}$
	V_y	$-1.3530263187520 \times 10^{-2}$	$-1.3530152097744 \times 10^{-2}$	$-1.3530828362023 \times 10^{-2}$
	V_z	$-5.6998631854817 \times 10^{-3}$	$-5.6998163886731 \times 10^{-3}$	$-5.7001012664635 \times 10^{-3}$

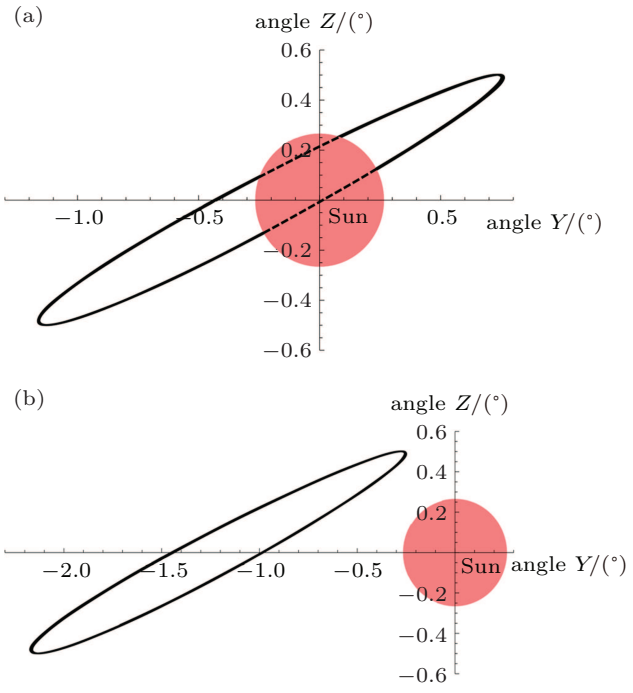


Fig. 2. (color online) S/C1 view form Earth before rotating the initial conditions by an angle (a) and after rotating by an angle 2.0° (b) for the case of inclination angle 1.0°.

3.3. Method of optimization

Our optimization method is to modify the initial velocities and initial heliocentric distances to reach the aim of (i) equalizing the three arm lengths of the ASTROD-GW formation as much as possible and (ii) reducing the relative Doppler velocities between three pairs of spacecrafts as much as possible.

During the actual optimization procedure, we use the following equation to modify the average period of the orbit:

$$\boldsymbol{V}_{\rm new} = \boldsymbol{V}_{\rm prev} + \Delta\boldsymbol{V} \approx \left(1 - \frac{1}{3}\frac{\Delta T}{T}\right)\boldsymbol{V}_{\rm prev}. \tag{12}$$

For the case of inclination angle of 1°, we calculate the 3 S/Cs orbits with the initial choice of initial conditions listed in column 3 of Table 2 using the CGC 2.7.1 ephemeris. The average periods of the 3 S/Cs in 10 years are 365.256 days (S/C1), 365.267 days (S/C2), and 365.266 days (S/C3) respectively. We use Eq. (12) to change the initial velocities so that the average period of S/C1, S/C2 and S/C3 is adjusted to 365.255 days, 365.257 days, and 365.257 days respectively. The initial conditions after this step are listed in column 4 of Table 2. In

the next step, we use the following equations to trim the S/C eccentricities to be nearly circular:

$$\begin{aligned} \boldsymbol{R}_{\rm new} &= \boldsymbol{R}_{\rm prev} + \Delta\boldsymbol{R} \approx \left(1 + \frac{\Delta R}{R}\right)\boldsymbol{R}_{\rm prev}, \\ \boldsymbol{V}_{\rm new} &= \boldsymbol{V}_{\rm prev} + \Delta\boldsymbol{V} \approx \left(1 - \frac{\Delta R}{R}\right)\boldsymbol{V}_{\rm prev}. \end{aligned} \tag{13}$$

Here, R is the initial heliocentric distance of spacecraft. The fractional adjustment $\pm(\Delta R/R)$ in $\boldsymbol{R}_{\rm prev}$ and $\boldsymbol{V}_{\rm prev}$ would adjust eccentricity without adjust the period of the orbit. The initial conditions after all optimization are listed in column 5 of Table 2.

As for the inclination angle is 0.0°, 0.5°, 1.5°, 2°, 2.5°, and 3°, the optimization processes are similar to the inclination is 1.0°.

The variation of arm lengths, difference of arm lengths, angles between arms, velocities in the measure direction, inclination of the unit normal $\boldsymbol{n}$ of the ASTROD-GW formation and azimuthal angle of $\boldsymbol{n}$ in 10 years are illustrated for the case with the orbit inclination angle 1° as shown in Figs. 3(a)–3(f), respectively. For this and other inclination cases, their values of Doppler velocity variations and arm length variations in 10 years are listed in columns 5 and 6 of Table 1 for comparison.

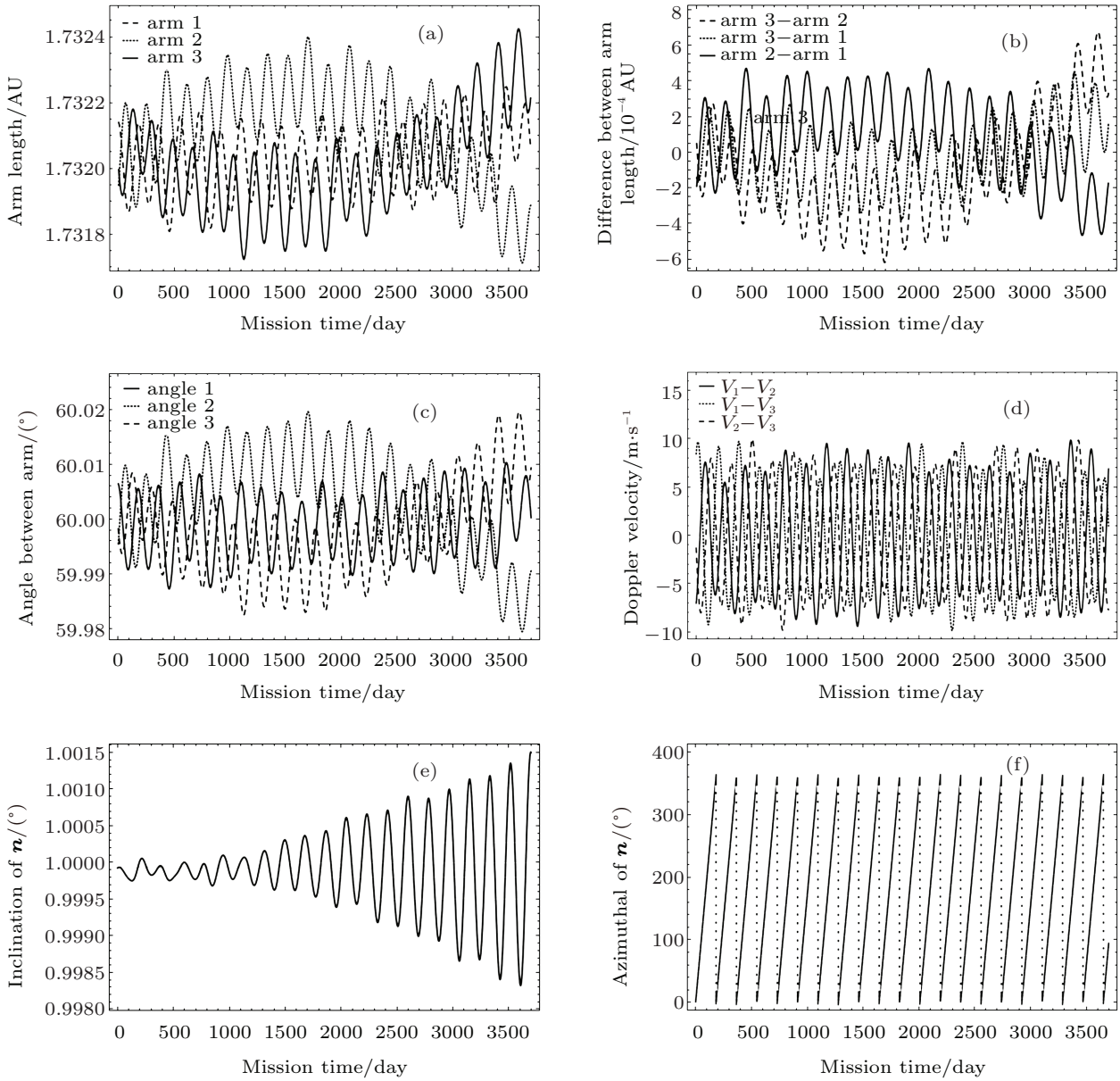


Fig. 3. The variation of (a) arm lengths, (b) difference of arm lengths, (c) angles between arms, (d) velocities in the measure direction, (e) inclination of the unit normal $\boldsymbol{n}$ of the ASTROD-GW formation and (f) azimuthal angle of $\boldsymbol{n}$ in 10 years for the case with the orbit inclination angle 1°.

3.4. Results of optimization

The initial positions and initial velocities of the 3 spacecrafts obtained after the optimization processes of Section 3.3 in J2000 equatorial solar-system barycentric coordinate system for the inclination angle 0°, 0.5°, 1°, 1.5°, 2°, 2.5°, and 3° are listed in the fourth-to-sixth columns of Table 3.

Table 3. Initial states of S/Cs at epoch JD2464500.0 for the 3 S/Cs after optimizations in J2000 equatorial solar-system-barycentric coordinate system for the inclination angle $\lambda = 0.0°$, $0.5°$, $1.0°$, $1.5°$, $2.0°$, $2.5°$, and $3.0°$ respectively.

λ			S/C1	S/C2	S/C3
		X	$-4.2796878676817\times10^{-2}$	$8.8117798070826\times10^{-1}$	$-8.4947241483190\times10^{-1}$
	initial position/AU	Y	$9.1125233495679\times10^{-1}$	$-4.3287312094977\times10^{-1}$	$-4.9495904068582\times10^{-1}$
		Z	$3.9520005050495\times10^{-1}$	$-1.8754965452141\times10^{-1}$	$-2.1446719503333\times10^{-1}$
0.0°		V_x	$-1.7183095034183\times10^{-2}$	$8.0177988365537\times10^{-3}$	$9.1828142475163\times10^{-3}$
	initial velocity/(AU/day)	V_y	$-6.2194110283150\times10^{-4}$	$1.3961176877644\times10^{-2}$	$-1.3355134639207\times10^{-2}$
		V_z	$-2.6979249323306\times10^{-4}$	$6.0527629379897\times10^{-3}$	$-5.7903075201295\times10^{-3}$
		X	$-3.5819911669671\times10^{-2}$	$8.7790469169867\times10^{-1}$	$-8.5317761553607\times10^{-1}$
	initial position/AU	Y	$9.1143723606865\times10^{-1}$	$-4.3549057022393\times10^{-1}$	$-4.9250178488352\times10^{-1}$
		Z	$3.9537317729935\times10^{-1}$	$-1.9696765577002\times10^{-1}$	$-2.0521201708840\times10^{-1}$
0.5°		V_x	$-1.7186887468334\times10^{-2}$	$8.1238999308544\times10^{-3}$	$9.0809973986794\times10^{-3}$
	initial velocity/(AU/day)	V_y	$-4.5210095520829\times10^{-4}$	$1.3879665203167\times10^{-2}$	$-1.3443438367041\times10^{-2}$
		V_z	$-3.5976439874011\times10^{-4}$	$6.0978417340874\times10^{-3}$	$-5.7453995292536\times10^{-3}$
		X	$-2.8842514605546\times10^{-2}$	$8.7453598387569\times10^{-1}$	$-8.5679330969623\times10^{-1}$
	initial position/AU	Y	$9.1158659433458\times10^{-1}$	$-4.3802677355114\times10^{-1}$	$-4.8995800210059\times10^{-1}$
		Z	$3.9553088730467\times10^{-1}$	$-2.0634980179207\times10^{-1}$	$-1.9591994878015\times10^{-1}$
1.0°		V_x	$-1.7188363750567\times10^{-2}$	$8.2301033726700\times10^{-3}$	$8.9792464008067\times10^{-3}$
	initial velocity/(AU/day)	V_y	$-2.8220098038726\times10^{-4}$	$1.3797253460590\times10^{-2}$	$-1.3530828362023\times10^{-2}$
		V_z	$-4.4969796642665\times10^{-4}$	$6.1425244722884\times10^{-3}$	$-5.7001012664635\times10^{-3}$
		X	$-2.5354637468848\times10^{-2}$	$8.7277485656422\times10^{-1}$	$-8.5853944803538\times10^{-1}$
	initial position/AU	Y	$9.1162752109802\times10^{-1}$	$-4.3768521777563\times10^{-1}$	$-4.9008352249095\times10^{-1}$
		Z	$3.9564157234190\times10^{-1}$	$-2.1448302499827\times10^{-1}$	$-1.8778616669275\times10^{-1}$
1.5°		V_x	$-1.7186475849607\times10^{-2}$	$8.2836295551138\times10^{-3}$	$8.9286603191558\times10^{-3}$
	initial velocity/(AU/day)	V_y	$-1.6734353206691\times10^{-4}$	$1.3740218938950\times10^{-2}$	$-1.3588357937831\times10^{-2}$
		V_z	$-5.6346990499641\times10^{-4}$	$6.1981969674239\times10^{-3}$	$-5.6418723212812\times10^{-3}$
		X	$-1.8377019454199\times10^{-2}$	$8.6928410315028\times10^{-1}$	$-8.6202745951776\times10^{-1}$
	initial position/AU	Y	$9.1170983137539\times10^{-1}$	$-4.4008950965408\times10^{-1}$	$-4.8739932270530\times10^{-1}$
		Z	$3.9577017809207\times10^{-1}$	$-2.2380515792750\times10^{-1}$	$-1.7843625650587\times10^{-1}$
2.0°		V_x	$-1.7184087416603\times10^{-2}$	$8.3897932228791\times10^{-3}$	$8.8269105632561\times10^{-3}$
	initial velocity/(AU/day)	V_y	$2.5668890281350\times10^{-6}$	$1.3655647257599\times10^{-2}$	$-1.3673677978699\times10^{-2}$
		V_z	$-6.5333704018832\times10^{-4}$	$6.2419097897323\times10^{-3}$	$-5.5957087504276\times10^{-3}$
		X	$-1.6635186808372\times10^{-2}$	$8.6826941613519\times10^{-1}$	$-8.6277837376267\times10^{-1}$
	initial position/AU	Y	$9.1169794863181\times10^{-1}$	$-4.3822782009220\times10^{-1}$	$-4.8877342743721\times10^{-1}$
		Z	$3.9585791785736\times10^{-1}$	$-2.3127457630524\times10^{-1}$	$-1.7084833096099\times10^{-1}$
2.5°		V_x	$-1.7178593572115\times10^{-2}$	$8.4175795794339\times10^{-3}$	$8.8025653512540\times10^{-3}$
	initial velocity/(AU/day)	V_y	$8.9879005834072\times10^{-5}$	$1.3610739355664\times10^{-2}$	$-1.3715709566895\times10^{-2}$
		V_z	$-7.7896390115972\times10^{-4}$	$6.3028004648275\times10^{-3}$	$-5.5308031306408\times10^{-3}$
		X	$-1.4894058497576\times10^{-2}$	$8.6722736973803\times10^{-1}$	$-8.6349420788078\times10^{-1}$
	initial position/AU	Y	$9.1168328063245\times10^{-1}$	$-4.3631776883318\times10^{-1}$	$-4.9009275125682\times10^{-1}$
		Z	$3.9594441468004\times10^{-1}$	$-2.3872020555868\times10^{-1}$	$-1.6323977249558\times10^{-1}$
3.0°		V_x	$-1.7171754206138\times10^{-2}$	$8.4455810575003\times10^{-3}$	$8.7785311071194\times10^{-3}$
	initial velocity/(AU/day)	V_y	$1.7717529782666\times10^{-4}$	$1.3565154450644\times10^{-2}$	$-1.3757170437319\times10^{-2}$
		V_z	$-9.0453594279848\times10^{-4}$	$6.3633637953983\times10^{-3}$	$-5.4656812863068\times10^{-3}$

4. Time-delay interferometry (TDI)

For laser-interferometric antenna for space detection of GWs, the arm lengths vary according to orbit dynamics. In order to attain the requisite sensitivity, laser frequency noise must be suppressed below the secondary noises such as the optical path noise, acceleration noise, etc. For suppressing laser frequency noise, it's necessary to use time delay interferometry in the analysis to match the optical path length of different beams. The better match of the optical path lengths are, the better cancellation of the laser frequency noise and the easier to achieve the requisite sensitivity. In case of exact match, the laser frequency noise is fully cancelled, as in the original Michelson interferometer.

4.1. Basics of time delay interferometry

The TDI was first used in the study of ASTROD mission concept.[27,28,46] In the deep-space interferometry, long distances are invariably involved. Due to long distances, laser light is attenuated to a great extent at the receiving spacecraft. To transfer the laser light back or to another spacecraft, amplification is needed. The procedure is to phase lock the local laser to the incoming weak laser light and to transmit the local laser light back to another spacecraft. We have demonstrated the phase locking of a local oscillator with 2-pW laser light in

laboratory.[47,48] Dick *et al.*[49] have demonstrated phase locking to 40-fW incoming weak laser light. The power requirement feasibility for ASTROD-GW is met with these developments. In the 1990s, we used the following two TDI configurations during the study of ASTROD interferometry and obtained numerically the path length differences using the Newtonian dynamics[27,28]

i) unequal arm Michelson TDI configuration

Path 1: S/C1 → S/C2 → S/C1 → S/C3 → S/C1,

Path 2: S/C1 → S/C3 → S/C1 → S/C2 → S/C1;

ii) Sagnac TDI configuration

Path 1: S/C1 → S/C2 → S/C3 → S/C1,

Path 2: S/C1 → S/C3 → S/C2 → S/C1.

Here, we do the same thing for ASTROD-GW with inclined orbit. For the numerical evaluation, we take a common receiving time epoch for both beams; the results would be very close to each other numerically if we take the same start time epoch and calculate the path differences. The results of this calculation for orbit configuration with 1° inclination are shown in Fig. 4. We refer to the path S/C1 → S/C2 → S/C1 as a and the path S/C1 → S/C3 → S/C1 as b. Hence the difference ΔL between Path 1 and Path 2 for the unequal-arm Michelson can be denoted as $ab - ba \equiv [a, b]$.

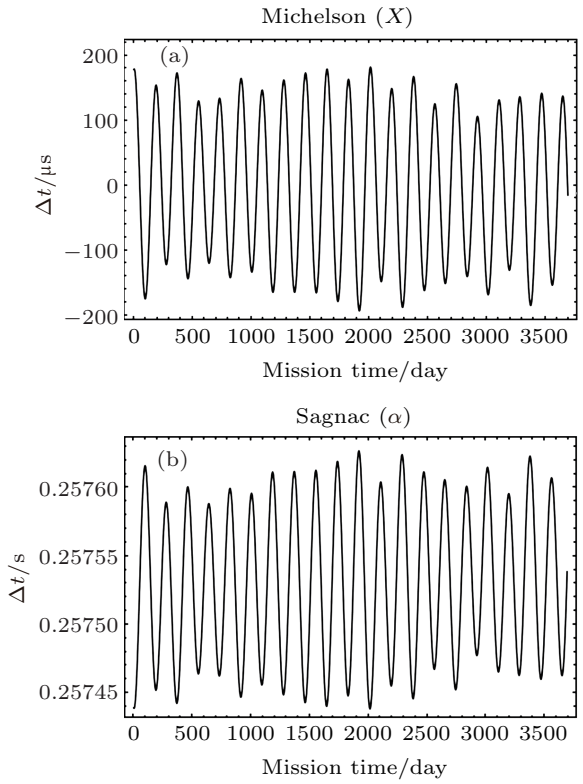


Fig. 4. Path length differences between two optical paths of the Unequal-arm Michelson TDI configuration (X) (a) and Sagnac TDI configuration (α) (b) for ASTROD-GW orbit formation with 1° inclination.

Time delay interferometry has been investigated for LISA much more thoroughly since 1999.[29,30] The first-generation and second-generation TDIs are proposed. In the first generation TDIs, static situations are considered. While in the second generation TDIs, motions are compensated to a certain degree. The two configurations considered above (Fig. 4) belong to the first generation TDI configurations. We shall not review more about these historical developments here, but the readers may refer to the excellent review by Tinto and Dhurandhar[30] for comprehensive treatment.

4.2. First-generation time delay interferometry

The first-generation TDIs include Sagnac (α, β, γ), Unequal-arm Michelson (X, Y, Z), Relay (U, V, W), Beacon (P, Q, R), and Monitor (E, F, G) configurations. The geometric representation of these TDIs according to Vallisneri[50] is shown in Fig. 5. Each type has three sub-types based on the different initial points of spacecraft. The path length differences for the Michelson-X TDI configuration and Sagnac-α TDI configuration are shown in Fig. 4 of Section 4.1 for ASTROD-GW orbit formation with 1° inclination. Those for Relay-U, Beacon-P, and Monitor-E are shown in Fig. 6.

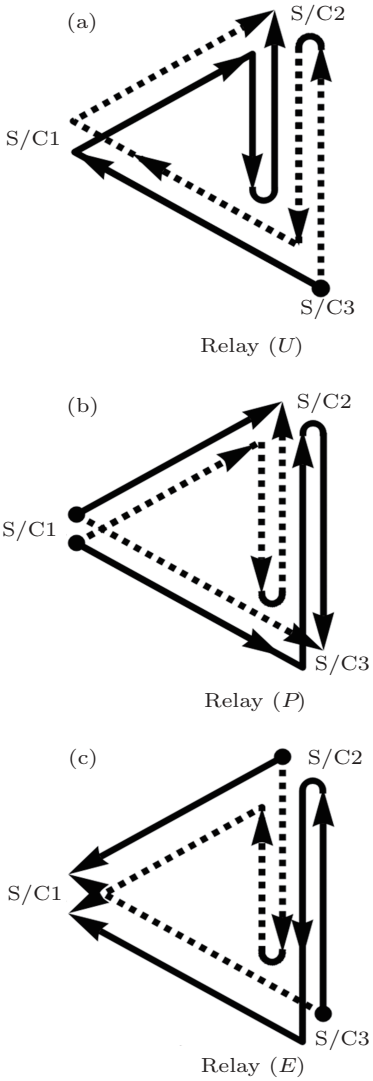


Fig. 5. Interference paths of the 1st-generation time-delay interferometry for Relay (U) (a), Beacon (P) (b), and Monitor E (c).

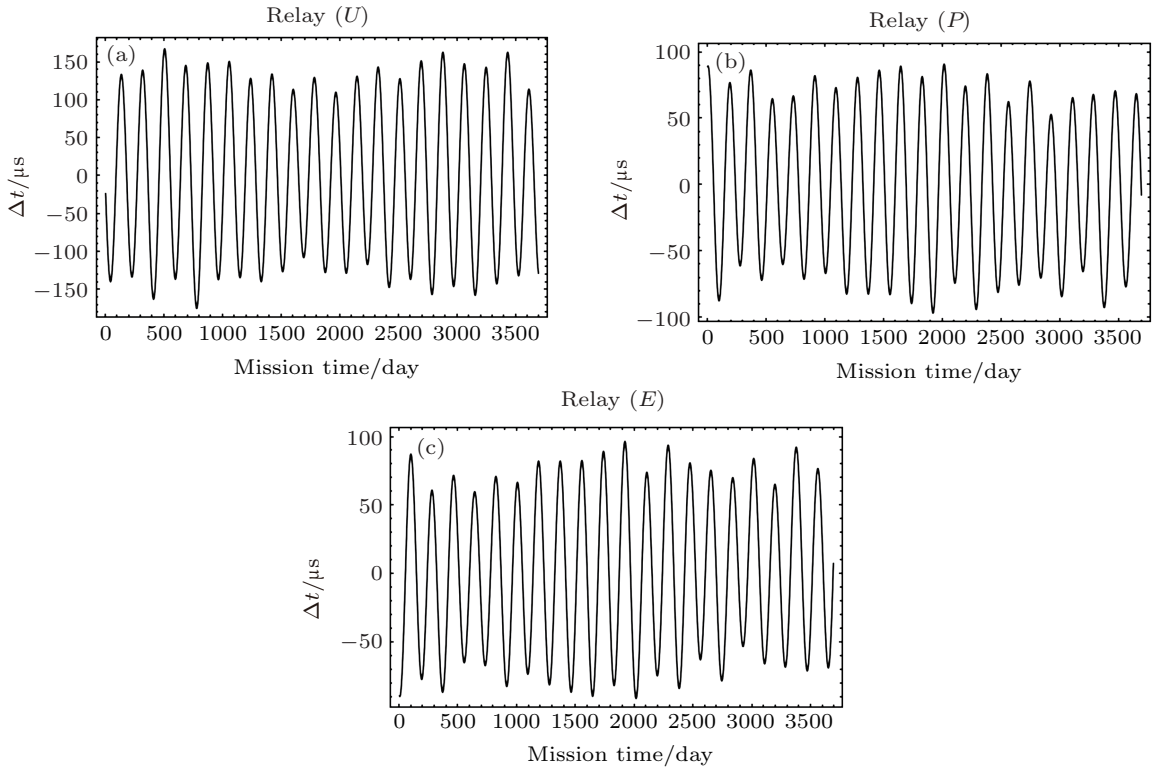


Fig. 6. Path length differences between two optical paths of the Relay-U (a), Beacon-P (b), and Monitor-E (c) TDI configurations for ASTROD-GW orbit formation with 1° inclination.

4.3. Second-generation TDIs in the case of one interferometric detector with two arms

As in our previous paper,[34] we calculated the TDI path length differences for the second-generation TDIs in the case of one detector with two arms obtained by Dhurandhar *et al.*[51] These configurations are listed in degree-lexicographic order as follows:

(I) $n = 1$, $[ab, ba] = abba - baab$,

(II) $n = 2$, $[a^2b^2, b^2a^2]$, $[abab, baba]$; $[ab^2a, ba^2b]$,

(III) $n = 3$, $[a^3b^3, b^3a^3]$, $[a^2bab^2, b2aba^2]$, $[a^2b^2ab, b^2a^2ba]$, $[a^2b^3a, {}^2a^3b]$, $[aba^2b^2, bab^2a^2]$, $[ababab, bababa]$, $[abab^2a, baba^2b]$, $[ab^2a^2b, ba^2b^2a]$, $[ab^2aba, ba^2bab]$, $[ab^3a^2, ba^3b^2]$, lexicographic (binary) order.

We take a common receiving time epoch for both beams and calculate the path differences. Figure 7 shows the numerical results for the $n = 1$ and $n = 2$ TDI configurations for the ASTROD-GW orbit configuration with 1° inclination. Table 4 compiles the rms path length differences of all TDI configurations listed above for various degrees of ASTROD-GW formation inclination (0°, 0.5°, 1°, 1.5°, 2°, 2.5°, and 3°) with respect to the ecliptic plane.

Table 4. Compilation of the rms path length differences of various first generation TDI configurations for various degrees of ASTROD-GW formation inclination (0°, 0.5°, 1°, 1.5°, 2°, 2.5°, and 3°) with respect to the ecliptic plane.

TDI	ASTROD-GW TDI path difference ΔL						
configuration	0°[μs]	0.5°[μs]	1°[μs]	1.5°[μs]	2.0°[μs]	2.5°[μs]	3.0°[μs]
Michelson-X	24	34	111	249	443	692	997
Michelson-Y	18	35	113	251	444	692	996
Michelson-Z	23	36	115	253	447	697	1002
Sagnac-α	257610	257590	257531	257432	257293	257115	256898
Sagnac-β	257608	257588	257529	257431	257294	257118	256902
Sagnac-γ	257607	257588	257530	257432	257297	257122	256909
Relay-U	17	31	100	219	387	602	866
Relay-V	18	29	96	216	383	598	861
Relay-W	21	30	98	217	385	602	867
Beacon-P	12	17	56	125	222	346	499
Beacon-Q	9	18	57	136	222	346	498
Beacon-R	12	18	58	127	224	349	501
Monitor-E	12	17	56	125	222	346	499
Monitor-F	9	18	57	136	222	346	498
Monitor-G	12	18	58	127	224	349	501

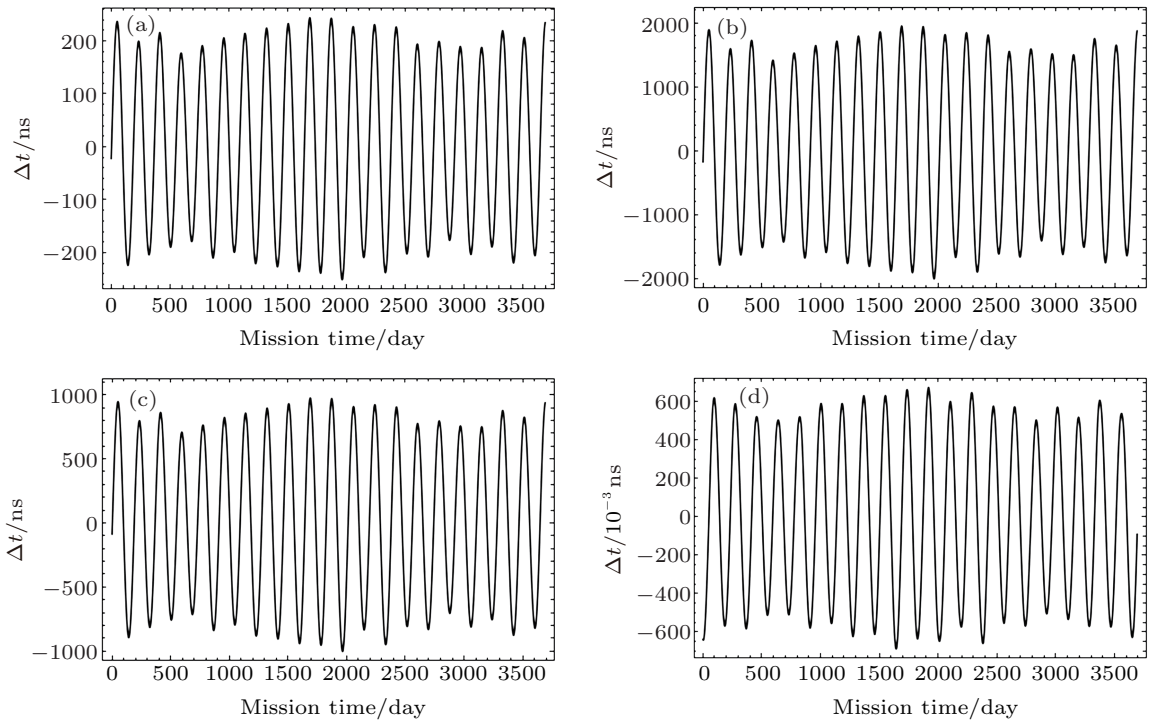


Fig. 7. Path length differences between two optical paths of second generation TDIs $n = 1$ and $n = 2$ TDI configurations for ASTROD-GW orbit formation with 1° inclination. (a) $[ab, ba]$, (b) $[a^2b^2, b^2a^2]$, (c) $[abab, baba]$, (d) $[ab^2a, ba^2b]$.

5. Discussion

We have optimized a set of 10-year inclined ASTROD-GW science mission orbits numerically using ephemeris framework starting at June 21, 2035, including cases of inclination angle is 0° (no inclination), 0.5°, 1.0°, 1.5°, 2.0°, 2.5°, and 3.0°. The purpose of inclined orbit is to resolve the binary reflection ambiguity and to enhance the polar resolution. We calculate optical path length difference of various first-generation and second-generation TDIs. The original ASTROD-GW path length difference requirement is 1.5 μs; this is equivalent to rms requirement of 1 μs. (From our calculation the absolute value of maximum difference is 1.4–1.5 times the rms in 10 years except in the Sagnac TDI configuration. If Sagnac configuration needs to be used to extract GW information, more requirements are needed. We will address to this issue in the future.) Compared to this original ASTROD-GW path length difference requirement of 1 μs rms, we have the following results.

(i) All the second-generation TDIs considered for one-detector case with no inclination and with 0.5° inclination satisfy this requirement (except in the marginal case $[a^3b^3, b^3a^3]$, the rms path length is 1.106 μs) (Table 5).

(ii) For the case of 1.0° inclination, of the 14 second-generation TDIs calculated, 6 satisfy the requirement (Table 5).

Table 5. Compilation of the rms path length differences of various TDI configurations in the case of one interferometric detector with two arms (vertex at S/C1) for various degrees of ASTROD-GW formation inclination (0°, 0.5°, 1°, 1.5°, 2°, 2.5°, and 3°) with respect to the ecliptic plane. [Nominal ASTROD-GW arm length: 260 Gm].

TDI configuration		ASTROD-GW TDI path difference ΔL						
		0°[ns]	0.5°[ns]	1°[ns]	1.5°[ns]	2.0°[ns]	2.5°[ns]	3.0°[ns]
$n = 1$	$[ab, ba]$	22	41	152	342	608	951	1370
	$[a^2b^2, b^2a^2]$	173	328	1209	2729	4862	7605	10957
$n = 2$	$[abab, baba]$	87	164	605	1365	2431	3803	5479
	$[ab^2a, ba^2b]$	0.0536	0.112	0.417	0.942	1.68	2.63	3.78
	$[a^3b^3, b^3a^3]$	582	1106	4079	9208	16407	25667	36980
	$[a^2bab^2, b^2aba^2]$	453	860	3172	7162	12761	19964	28762
	$[a^2b^2ab, b^2a^2ba]$	323	615	2266	5116	9115	14260	20544
	$[a^2b^3a, b^2a^3b]$	194	369	1360	3070	5469	8556	12327
	$[aba^2b^2, bab^2a^2]$	323	615	2266	5116	9115	14260	20545
$n = 3$	$[ababab, bababa]$	194	369	1360	3070	5469	8556	12327
	$[abab^2a, baba^2b]$	65	123	454	1024	1823	2852	4109
	$[ab^2a^2b, ba^2b^2a]$	65	123	454	1024	1823	2852	4109
	$[ab^2aba, ba^2bab]$	65	123	454	1024	1823	2852	4109
	$[ab^3a^2, ba^3b^2]$	194	369	1360	3070	5469	8556	12327

(iii) For the cases of 1.5° to 3°, the requirement needs to be relaxed by 10 to 37 times; that is the laser frequency stabilization noise need to be suppressed by this additional factor (Table 5).

(iv) Among the first-generation TDIs considered, the requirement for unequal arm Michelson, Relay, Beacon, and Monitor needs to be relaxed by 2–3 orders (Table 4).

(v) Experimental demonstration of TDI in laboratory for LISA has been implemented in 2010.[52] eLISA and the original ASTROD-GW TDI requirement are based on LISA requirement, and hence also demonstrated. With the present pace of development in laser technology, the laser frequency noise requirement is expected to be able to compensate for 2–3 order TDI requirement relaxation in 20 years.

(vi) X-configuration TDI sensitivity for GW sources has been studied extensively for eLISA.[18] It satisfies the present technological requirements well. With enhanced laser technology expected, it would also be good to study for ASTROD-GW. The study for GW sensitivity and GW sources for other first-generation and second-generation TDIs would also be encouraged.

References

[1] Ni W T 2010 *Mod. Phys. Lett. A* **25** 922
[2] *Classification of Gravitational Waves* http://astrod.wikispaces.com/file/view/GW-classification.pdf
[3] Hanson D, Hoover S, Crites A, *et al*. (SPTpol Collaboration) 2013 *Phys. Rev. Lett.* **111** 141301
[4] Ade P A R, Akiba Y, Anthony A E, *et al*. (POLARBEAR Collaboration) 2014 *Astrophys. J.* **794** 171
[5] Ade P A R, Aikin R W, Barkats D, *et al*. (BICEP2 Collaboration) 2014 *Phys. Rev. Lett.* **112** 241101
[6] Ade P A R, Aghanim N, Armitage-Caplan C, *et al*. (Planck Collaboration) 2014 *Astron. Astrophys.* **571** A16
[7] Naess S, Hasselfield M, McMahon J, *et al*. 2014 *JCAP* **10** 007
[8] The Advanced LIGO Team http://www.ligo.caltech.edu/advLIGO/
[9] The Advanced Virgo Team http://wwwcascina.virgo.infn.it/advirgo/docs/whitepaper.pdf
[10] *KAGRA Large-Scale Cryogenic Gravitational Wave Telescope Project* http://gwcenter.icrr.u-tokyo.ac.jp/en/
[11] *LIGO-India Moving Forward* http://www.phy.olemiss.edu/GR/?x=entry:entry120329-132004
[12] Unnikrishnan C S 2013 *Int. J. Mod. Phys. D* **22** 1341010
[13] *International Pulsar Timing Array* http://www.ipta4gw.org/
[14] *European Pulsar Timing Array (EPTA)* http://www.epta.eu.org/
[15] *North American Nanohertz Observatory for Gravitational Waves (NANOGrav)* http://www.nanograv.org/
[16] *Parkes Pulsar Timing Array (PPTA)* http://www.atnf.csiro.au/research/pulsar/ppta/
[17] Ni W T 2013 *Adv. Space Res.* **51** 525
[18] eLISA/NGO Assessment Study Team 2011 ESA/SRE 19 http://elisa-ngo.org/
[19] Ni W T 2009 *ASTROD Optimized for Gravitational-Wave Detection: ASTROD-GW–a pre-Phase A study proposal submitted to Chinese Academy of Sciences*, February 26, 2009
[20] Ni W T, Men J R, Mei X H, *et al*. 2009 *Proceedings of Sixth Deep Space Exploration Technology Symposium*, December 3–6, 2009, Sanya, China, p. 122
[21] Ni W T 2013 *Int. J. Mod. Phys. D* **22** 1341004
[22] Ni W T 2009 *Class. Quantum Grav.* **26** 075021
[23] Crowder J and Cornish N J 2005 *Phys. Rev. D* **72** 083005
[24] Kawamura S, Nakamura T, Ando M, *et al*. 2006 *Class. Quantum Grav.* **23** S125
[25] Kawamura S, Ando M, Seto N, *et al*. 2011 *Class. Quantum Grav.* **28** 094011
[26] Ando M and the DECIGO Working Group 2013 *Int. J. Mod. Phys. D* **22** 1341002
[27] Ni W T, Shy J T, Tseng S M, Xu X, Yeh H C, Hsu W Y, Liu W L, Tzeng S D, Fridelance P, Samain E and Wu A M 1997 *Proceedings of SPIE* 3116*: Small Spacecraft, Space Environments, and Instrumentation Technologies* p. 105
[28] Ni W T, Sandford M C W, Veillet C, Wu A M, Fridelance P, Samain E, Spalding G and Xu X 2003 *Adv. Space Res.* **32** 1437
[29] Armstrong J W, Estabrook F B and Tinto M 1999 *Astrophys. J.* **527** 814
[30] Tinto M and Dhurandhar S V 2005 *Living Rev. Relativity* **8** 4
[31] Wang G and Ni W T 2011 *Acta Astron. Sin.* **52** 427 (in Chinese)
[32] Wang G and Ni W T 2012 *Chin. Astron. Astrophys.* **36** 211
[33] Wang G 2011 *Time-delay Interferometry for ASTROD-GW* (MS Thesis) (Nanjing: Purple Mountain Observatory) (in Chinese)
[34] Wang G and Ni W T 2013 *Chin. Phys. B* **22** 049501
[35] Dhurandhar S V, Ni W T and Wang G 2013 *Adv. Space Res.* **51** 198
[36] Wang G and Ni W T 2013 *Class. Quantum Grav.* **30** 065011
[37] http://www.esa.int/Our_Activities/Space_Science/ESA_s_new_vision-_to_study_the_invisible_Universe
[38] Men J R, Ni W T and Wang G 2009 *Acta Astron. Sin.* **51** 198 (in Chinese)
[39] Men J R, Ni W T and Wang G 2010 *Chin. Astron. Astrophys.* **34** 434
[40] Yi Z 2002 *Publications of the Yunnan Observatory* **3** 9 (in Chinese)
[41] Damour, T, Soffel M and Xu C 1991 *Phys. Rev. D* **43** 3273
[42] Soffel M, Klioner S A, Petit G, Wolf P, Kopeikin S M, Bretagnon P, Brumberg V A, Capitaine N, Damour T, Fukushima T, Guinot B, Huang T, Lindegren L, Ma C, Nordtvedt K, Ries J, Seidelmann P K, Vokrouhlicky D, Will C and Xu C 2003 *Astron. J.* **126** 2687
[43] Brumberg V A 1991 *Essential Relativistic Celestial Mechanics* (Bristol: Adam Hilger) p. 175
[44] *The Asteroid Orbital Elements Database* ftp://ftp.lowell.edu/pub/elgb/astorb.html
[45] Folkner W M, Williams J G, Boggs D H, *et al.* 2014 *IPN Progress Report* **42** 196
[46] Ni W T 1997 *Gravitational Wave Detection* (Tokyo: Universal Academy Press) p. 117
[47] Liao A C, Ni W T and Shy J T 2002 *Publications of the Yunnan Observatory* **3** 88 (in Chinese)
[48] Liao A C, Ni W T and Shy J T 2002 *Int. J. Mod. Phys. D* **11** 1075
[49] Dick G J, Strekalov M D, Birnbaum K, *et al.* 2008 *IPN Progress Report* **42** 175
[50] Vallisneri M 2005 *Phys. Rev. D* **72** 042003
[51] Dhurandhar S V, Nayak K R and Vinet J Y 2010 *Class. Quantum Grav.* **27** 135013
[52] de Vine G, Ware B, McKenzie K, Spero R E, Klipstein W M and Shaddock D A 2010 *Phys. Rev. Lett.* **104** 211103